Liquid meniscus oscillation and drop ejection by ac voltage, pulsed dc voltage, and superimposing dc to ac voltages

Si Bui Quang Tran, Doyoung Byun,[*] Vu Dat Nguyen, and Tae Sam Kang

Department of Aerospace Information Engineering, Konkuk University, Seoul 143-701, Republic of Korea

(Received 18 January 2009; revised manuscript received 1 May 2009; published 31 August 2009)

The electrohydrodynamic (EHD) spraying technique has been utilized in applications such as inkjet printing and mass spectrometry technologies. In this paper, the role of electrical potential signals in jetting and on the oscillation of the meniscus is evaluated. The jetting and the meniscus oscillation behavior are experimentally investigated under ac voltage, ac voltage superimposed on dc voltage, and pulsed dc voltage. Based on this in-depth study of the meniscus behavior under various signals, the optimal signal is implemented to an EHD inkjet head for drop-on-demand operation. For applied ac voltage and ac voltage superimposed on dc voltage, the jetting phenomenon is a dynamic process due to sequential opposite sign signals. The jetting occurs at the end of the oscillation cycle, where the meniscus oscillates upward and arrives at its highest position.

I. INTRODUCTION

Since Zeleny's first systematic study of the subject [1], the mechanism of electrohydrodynamic (EHD) spraying has been studied by many researchers [2–10] and applied to many endeavors and devices, such as microcolloid thrusters [11–13], mass spectrometry [14–16], inkjet printing [17–21], fabrication of microspheres of biological materials [22], direct handling of living cells [23], and film deposition [24]. In application of inkjet printing technology, the microdripping mode or pulsating discontinuous jetting modes [4] are required for drop-on-demand operations [20,21]. The drop-on-demand operation plays a key role in the patterning of some shapes in industrial applications. Using a square wave pulse generator superimposed on the bias voltage, drop-on-demand ejection of droplets was implemented and patterning was carried out using conductive silver ink [21]. An EHD inkjet device is composed of a source nozzle and an extraction electrode, with an electrical circuit between the nozzle and the electrode. A high voltage is applied between the nozzle and the extractor, producing a strong electric field around the tip of the nozzle. Accordingly, an electric charge is induced at the surface of the liquid meniscus to create an electric stress that stretches the meniscus in the direction of the field, and a droplet or jet of liquid is formed when the electrostatic force is stronger than the surface-tension force. Such an EHD printing has shown various advantages [17–21]. An EHD inkjet head can produce droplets smaller than the size of the nozzles that produce them. This unique feature distinguishes EHD printing from conventional methods by allowing a submicron resolution [18]. EHD printing has a great potential to offer complex and high-resolution printing. Existing studies of EHD printing have successfully demonstrated the drop-on-demand control of droplet ejection and various geometry buildups from dots and continuous lines that are possible through EHD [20,21]. The shape evolution of small droplets attached to a conducting surface and subjected to relatively strong electric fields is studied both experimentally and numerically, distinguishing equilibrium state, jetting state, and whole droplet jumping state [25]. However, most of the earlier works noted above used dc or pulsed dc voltage to form droplets, sprays, or electrospinning.

On the other hand, there are few studies on ac electrosprays, typically focusing on microdripping mode or pulsating jet mode. The few reported studies typically concentrated on generation of electrosprays at ac field without details of liquid meniscus oscillation or jetting mechanism and just applied to coatings [26,27]. And several studies investigated the effect of an ac component superimposed to top of a large dc signal on the production of uniform liquid droplets [28,29]. ac voltage coupled with dc voltage was applied to liquid jets in order to study the stability, the surface waves, and the resultant breakup process of the continuous liquid jet [8,30]. Jaworek *et al.* [8] focused on the effect of the viscosity of the liquid on the electrospray and concluded that the viscosity of the liquid plays a crucial role in synchronized spraying. The previous studies have not presented details of liquid meniscus oscillation on a nozzle tip or jet formation for the low-frequency regime (<2 kHz). ac voltage with a high frequency (>10 kHz) has also been used in electrospraying [31–35]. Lastochkin and Chang [31] described a mechanism of electrospraying with a high-frequency ac voltage. They attributed the spraying mechanism to a normal Maxwell force produced by an undispersed plasma cloud in front of the meniscus that produces a visible glow at the spherical tip. Yeo *et al.* [34] characterized ac spraying according to the amplitude and the frequency of the applied high-frequency ac field.

In this paper, to use ac voltage or ac voltage superimposed on a background dc voltage for an EHD drop-on-demand printing device, the behaviors of the liquid meniscus on a nozzle tip and jet formation at the apex of the meniscus are investigated according to the applied ac voltage, pulsed dc voltage, and ac voltage superimposed on a background dc voltage. Most existing EHD printing devices are based on dc voltage or pulsed dc voltage, which has several drawbacks when used with drop-on-demand printing. These include (1) dynamic instabilities due to meniscus elongation toward an

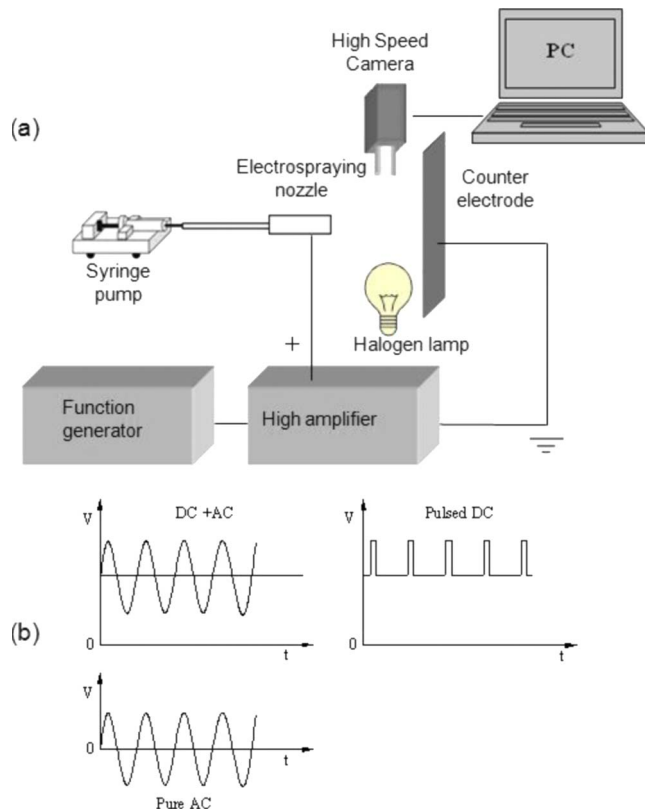*Corresponding author. FAX: +82 (2) 444-6670; dybyun@konkuk.ac.kr

FIG. 1. (Color online) Schematics of (a) experimental setup and (b) applied voltage signal.
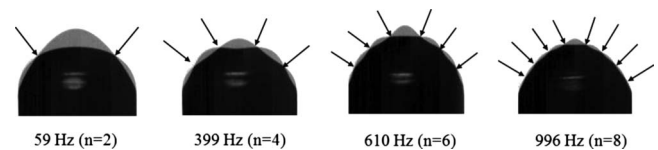

FIG. 2. Patterns of meniscus oscillation modes and resonance frequencies at 7.5, 8, 9, and 10.8 kVp-p voltages for modes 2, 4, 6, and 8, respectively.

nozzle. Three voltage signals of pure ac voltage, ac voltage superimposed on dc voltage, or pulsed dc voltage were applied between the nozzle and the extractor as shown in Fig. 1(b). The nozzle is located at distances of 8 or 11 mm from a counter-ground-electrode. The voltage signals are generated by a function generator (Agilent 33220A) and an amplifier (TREK 10/40A). The function generator can generate low voltage ac (20 Vp-p) or pulsed dc (10 V) signals while the amplifier can amplify the voltage up to 1000 times higher. A high-speed camera (Photron Ltd., Fastcam Ultima APX) with a microzoom lens and a halogen lamp was used to visualize the liquid meniscus behavior and jet formation. The high-speed camera is capable of imaging 4000 frames/s at a resolution of 512×512. For the jetting liquid, ethanol is used, whose physical properties are a density of 0.789 g/cm^3, a viscosity of 1.2 cP, an electrical conductivity of 0.0013 μS/cm, and a surface-tension coefficient of 22.8 dyn/cm. The liquid is supplied to the nozzle using a microsyringe pump (Harvard Co.) at a flow rate of 3 μl/min.

extraction electrode, resulting in liquid atomization; (2) electrical breakdown; and (3) droplet reflection or deflection due to same charges and resultant repulsive forces between the droplet and the substrate where other droplets are already deposited. Therefore, to tackle these drawbacks and to implement the ejection of droplets on demand, the effects of the three aforementioned signals are investigated and the ejection characteristics are compared. A series of experiments is conducted to characterize the effects of the frequency and the amplitude of ac and dc voltages on spraying. And the optimal oscillation frequency of ac voltage is suggested, which allows a more efficient ejection of droplets.

II. EXPERIMENTAL METHOD

Figure 1(a) shows a schematic of the experimental setup. An EHD device is composed of a source nozzle and an extraction electrode. The polymer-based [polymethyl methacrylate (PMMA)] nozzle was fabricated using a computer numerical control (CNC) mini engraving machine (MM-300S). The nozzle system contains a reservoir and a channel with a depth of 1 mm, a width of 1 mm, and a length of 40 mm. The protruding nozzle was fabricated using a CNC mini engraving machine (MM-300S), as the shape enhances the electric field at the tip and at the same time avoids wetting. The nozzle of the PMMA-based electrospray device has an inner diameter of 1 mm and an outer diameter of 1.5 mm. A high voltage was applied between the nozzle and the extractor, producing a strong electric field around the tip of the

III. RESULTS AND DISCUSSION

A. Effect of ac voltage

1. Meniscus oscillation without jetting

A series of experiments was conducted to evaluate the effect of ac voltage on meniscus behavior with and without jetting. First, an experiment was carried out to investigate the modes of oscillation under ac voltage. The distance between the electrode and the emitter was 11 mm. The liquid was supplied to the nozzle tip until the meniscus formed a hemisphere. The pump was then stopped to maintain the hemispherical shape of the meniscus. The applied voltage was gradually increased to a voltage sufficient for oscillation. Here, the focus is on even modes of oscillation, which implies that the meniscus oscillates axisymmetrically. The mode of oscillation is defined by the number of lobes on the meniscus.

Figure 2 shows the even oscillation modes and the experimental resonant frequencies. The resonant frequencies are determined by observing the oscillation of the meniscus while gradually increasing the applied frequency from 0 Hz to 2 kHz. At the resonant values of the applied frequency, the magnitude of the oscillation is maximized according to each oscillation mode. The oscillation at the lower modes required a lower supplied energy, i.e., a lower amplitude of the applied voltage. The appropriate voltage amplitudes for oscillation without jetting for modes 2, 4, 6, and 8 were determined to be 7.5, 8, 9, and 10.8 kVp-p, respectively. The

applied voltages were adjusted around the appropriate values to find the ranges of oscillation. The ranges are narrow, approximately 300 V around the appropriate values. When the voltage is low, the surface-tension force is highly dominant and the effect of the voltage is small. The meniscus maintains a hemispherical shape with a small amount of vibration. If the voltage is high, polarization on the meniscus can no longer be balanced by the surface-tension force. In such cases, the meniscus breaks up and ejection occurs. During the experiment, it was observed that the oscillation frequency is twice the applied frequency in mode 2 and is equal to the applied frequency in modes 4, 6, and 8.

Drop oscillation modes were also observed under ac electrowetting [35]. The electrowetting phenomenon is induced by the electric force concentrated on the three-phase contact line, and the meniscus moves freely due to the hydrophobic substrate. Wang *et al.* [36] studied the oscillation of a drop induced by a high-frequency (>10 kHz) ac electric field. They reported that a large droplet emerged from the nozzle and formed a nearly spherical shape. The drop can be considered a free spherical drop. The acting force is the Maxwell stress distributed on the surface of the meniscus. The authors of that study observed oscillation modes of 2–6. However, in this study, the drop is a constrained hemisphere due to the tip of the nozzle with the acting force being the Maxwell stress distributed on the surface of the meniscus. The pinning at the nozzle and the use of a different frequency might be the reasons for the different oscillation modes found in this study. This should be further investigated theoretically by building a mathematical model.

The oscillation of a constrained meniscus has been studied, but the electric field has not been considered. Strani and Sabetta [37] analyzed the axisymmetric free vibrations of a liquid drop in partial contact with a spherical bowl neglecting the effects of gravity and viscosity. The Green's-function method and the expansion of the velocity potentials in a series of Legendre polynomials were used to derive and reduce the problem to the solution of a single integral equation. Strani [38] studied the gravity capillary small vibrations of a fluid meniscus when the fluid was incompressible and inviscid. The fluid was contained in a trough, and the line of contact on the lateral walls was fixed. The vibration frequencies and modes were determined as eigenmodes and eigenvalues of a linear operator whose components were analytically given. De Bernardis and Strani [39] investigated the linear free vibration of the meniscus of a bulk inviscid fluid in a cylindrical duct with a fixed line of contact between the meniscus and the lateral walls. The gravity along the duct axis was taken into account. The problem was reduced to one of determining the eigenvalues and eigenvectors of a linear operator whose components are analytically evaluated. Bauer [40] solved the problem of liquid droplet oscillation of hemispherical and conical systems with anchored edges on a plate in zero gravity. The paper reported the resonant frequencies of even modes. However, there is no theoretical study on the oscillation of a liquid droplet, whose edges are anchored on a plate or a nozzle, considering the effect of an applied ac electric field.

Therefore, we present in this study a possible approach to the simulation of droplet oscillation under ac voltage. To
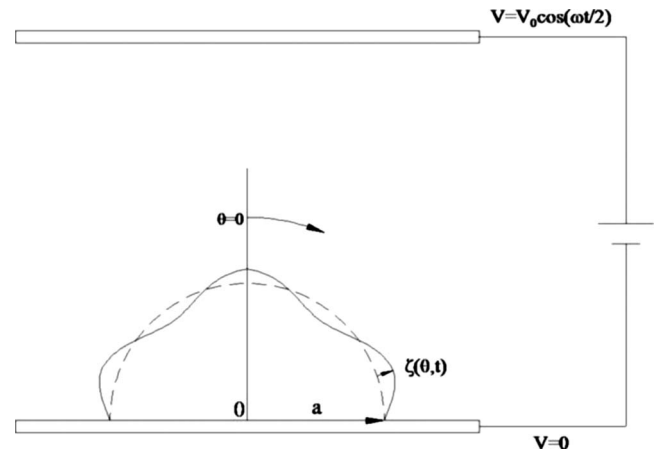

FIG. 3. Geometry and coordinates of the hemispherical meniscus on a conductive flat plate.

simplify the boundary condition, the oscillation of liquid droplet, with anchored edges and hemispherical meniscus on a conductive flat plate, is simulated under a uniform ac electric field as an example problem. This sample problem is very similar to the problem of a droplet on a nozzle without a boundary condition on a nozzle. The boundary condition at the interface between the droplet and the nozzle should be carefully modeled. A theory for the nozzle will be developed and applied in a future work.

Figure 3 shows the geometry and the spherical coordinate of the hemispherical meniscus on a conductive flat plate. It is assumed that the liquid is inviscid, incompressible, and perfect conductive in a zero-gravity environment. And it is assumed that the meniscus oscillates linearly. Then the Laplace equation of the velocity potential (ϕ) has to be solved for the liquid inside the meniscus [40],

$$\Delta \phi = 0. \tag{1}$$

The Laplace operator in spherical coordinate is given by

$$\Delta = \frac{1}{r^2} \frac{\partial}{\partial r} \left(r^2 \frac{\partial}{\partial r} \right) + \frac{1}{r^2 \sin \theta} \frac{\partial}{\partial r} \left(\sin \theta \frac{\partial}{\partial \theta} \right), \tag{2}$$

where r is a radius and θ is a polar angle. The boundary conditions are

$$\frac{\partial \phi}{r \, \partial \theta} = 0 \quad \text{on a substrate or } \theta = \pi/2 \tag{3}$$

and the free surface condition at $r=a$ is the kinematic condition

$$\frac{\partial \zeta}{\partial t} = \frac{\partial \phi}{\partial r}, \tag{4}$$

where a is an initial radius of a hemispherical meniscus and $\zeta(\theta, t)$ is free surface displacement. The dynamic condition for linear oscillation is as follows:

$$\frac{\sigma}{\rho a^2}\left[2\zeta + \frac{1}{\sin\theta}\frac{\partial}{\partial\theta}\left(\sin\theta\frac{\partial\zeta}{\partial\theta}\right)\right] = \left.\frac{\partial\phi}{\partial t}\right|_{r=a} + \frac{[\![T^e_{nn}]\!]}{\rho}, \quad (5)$$

where $[\![T^e_{nn}]\!]=\frac{1}{2}\varepsilon_0 E_n^2$ is the normal acting electric stress on the meniscus for perfect conductor liquid, ε_0 is the vacuum dielectric constant, E_n is the normal electric field, σ is the liquid surface tension, t is the time, and ρ is the liquid density. To include the effects of the external electric field, the normal acting electric stress term is added into the dynamic condition equation.

The anchored edge condition is as follows:

$$\zeta = 0 \quad \text{at} \quad \theta = \pm\pi/2 \quad \text{and} \quad r = a. \quad (6)$$

To calculate the normal acting electric stress, the electric potential field outside the meniscus should be obtained. The electric potential field (U) is governed by the Laplace equation,

$$\Delta U = 0. \quad (7)$$

The boundary conditions are

$$U(r,\theta,t) = 0 \quad \text{on the substrate} \quad \text{or} \quad \theta = \pm\pi/2, \quad (8)$$

$$U(r,\theta,t) = e^{i\omega t/2}E_0 r\cos\theta \quad (9)$$

as

$$r\to\infty, \quad \text{uniform electric field condition,}$$

$$U(r,\theta,t) = 0 \quad \text{on the free meniscus} \quad \text{or} \quad r = r_f, \quad (10)$$

where ω is the oscillation frequency, i is an imaginary unit, E_0 is the value of the uniform electric field, $r_f = a + \zeta(\theta,t)$ is the function indicating the meniscus shape, and r is the radial distance of the spherical coordinate.

The solving procedure for the velocity potential and the free surface displacement [Eqs. (1)–(4)] was presented by Bauer [40],

$$\zeta(\theta,t) = \sum_{n=1}^{\infty}\frac{2nA_n}{i\omega a}P_{2n}(\cos\theta)e^{i\omega t}, \quad (11)$$

$$\phi(r,\theta,t) = \sum_{n=1}^{\infty} e^{i\omega t}A_n\left(\frac{r}{a}\right)^{2n}P_{2n}(\cos\theta)e^{i\omega t}, \quad (12)$$

where A_n is an unknown coefficient and will be calculated from Eq. (5). The anchored edge condition in Eq. (6) is expressed as

$$\sum_{n=1}^{\infty}\frac{2nA_n}{i\omega a}P_{2n}(0) = 0, \quad (13)$$

$$P_{2n}(0) = \frac{(-1)^n(2n)!}{2^{2n}(n!)^2}. \quad (14)$$

Therefore, we have the following relation:

$$\sum_{n=1}^{\infty}\frac{2nA_n}{i\omega a}\frac{(-1)^n(2n)!}{2^{2n}(n!)^2} = 0. \quad (15)$$

The solution of electrical potential based on Eqs. (7)–(9) is

$$U(r,\theta,t) = \left[E_0 r\cos\theta + \sum_{k=1}^{\infty}\left(\frac{a}{r}\right)^{2k}B_k P_{2k-1}(\cos\theta)\right]e^{i\omega t/2}, \quad (16)$$

where $P_m(\cos\theta)$ is the Legendre polynomial function and B_k is an unknown coefficient. Equation (16) is the general solution of the Laplace equation [Eq. (7)]. At $\theta = \pm\pi/2$ or $\cos\theta = 0$, $P_{2k-1}(\cos\theta) = 0$, then $U(r,\pm\pi/2,t) = 0$. Furthermore, $U(r,\theta,t)\to e^{i\omega t/2}E_0 r\cos\theta$ as $r\to\infty$. Therefore, the solution in Eq. (16) satisfies Eqs. (7)–(9). The coefficient B_k will be solved by using the condition in Eq. (10).

The electric field affects the meniscus shape [Eq. (5)] and the meniscus shape affects the electric field distribution [Eq. (10)]. There is an interaction between the electric field and the hydrodynamic problems. Therefore, the whole problem should be solved iteratively.

Substituting Eq. (12) into Eq. (5) and dividing both sides by $e^{i\omega t}$ yield

$$\frac{1}{\sin\theta}\frac{\partial}{\partial\theta}\left(\sin\theta\frac{\partial\bar{\zeta}}{\partial\theta}\right) + 2n(2n+1)\bar{\zeta} + [2 - 2n(2n+1)]\bar{\zeta}$$

$$= \frac{i\omega\rho a^2}{\sigma}\sum_{n=1}^{\infty}A_n P_{2n}(\cos\theta) + \frac{a^2\varepsilon_0}{2\sigma}\bar{E}_n^2, \quad (17)$$

where $E_n = (\partial U/\partial r)n_r + (1/r)(\partial U/\partial\theta)n_\theta$ and n_r and n_θ are the components of the normal vector to the meniscus in the spherical coordinate. The general solution of this ordinary and inhomogeneous differential equation is presented by

$$\bar{\zeta} = \bar{\zeta}_0 + \bar{\zeta}_1 + \bar{\zeta}_2. \quad (18)$$

Here, $\bar{\zeta}_0$ is the solution of the homogeneous equation

$$\frac{1}{\sin\theta}\frac{\partial}{\partial\theta}\left(\sin\theta\frac{\partial\bar{\zeta}}{\partial\theta}\right) + 2n(2n+1)\bar{\zeta} + [2 - 2n(2n+1)]\bar{\zeta} = 0 \quad (19)$$

and $\bar{\zeta}_0$ is expressed as [40]

$$\bar{\zeta}_0 = A_0\cos\theta. \quad (20)$$

$\bar{\zeta}_1$ is the solution of the inhomogeneous equation

$$\frac{1}{\sin\theta}\frac{\partial}{\partial\theta}\left(\sin\theta\frac{\partial\bar{\zeta}}{\partial\theta}\right) + 2n(2n+1)\bar{\zeta} + [2 - 2n(2n+1)]\bar{\zeta}$$

$$= \frac{i\omega\rho a^2}{\sigma}\sum_{n=1}^{\infty}A_n P_{2n}(\cos\theta) \quad (21)$$

and $\bar{\zeta}_1$ is expressed as [40]

$$\bar{\zeta}_1 = -\frac{i\omega\rho a^2}{\sigma}\sum_{n=1}^{\infty}\frac{A_n}{2n(2n+1)-2}P_{2n}(\cos\theta). \quad (22)$$

$\bar{\zeta}_2$ is the solution of the inhomogeneous equation

$$\frac{1}{\sin\theta}\frac{\partial}{\partial\theta}\left(\sin\theta\frac{\partial\bar{\zeta}}{\partial\theta}\right)+2n(2n+1)\bar{\zeta}+[2-2n(2n+1)]\bar{\zeta}$$

$$=\frac{a^2\varepsilon_0}{2\sigma}\bar{E}_n^2 \quad (23)$$

and $\bar{\zeta}_2$ is expressed as

$$\bar{\zeta}_2 = \sum_{n=1}^{\infty}C_nP_{2n}(\cos\theta), \quad (24)$$

where C_n are the unknown coefficients.

Substituting Eq. (24) into Eq. (23) yields

$$\sum_{n=1}^{\infty}2n[2-2n(2n+1)]C_nP_{2n}(\cos\theta)=\frac{a^2\varepsilon_0}{2\sigma}\bar{E}_n^2. \quad (25)$$

The coefficients C_n are obtained by solving Eq. (25). By substituting Eqs. (20), (22), and (24) into Eq. (18), the general solution of Eq. (17) is given as

$$\bar{\zeta}=A_0\cos\theta-\frac{i\omega\rho a^2}{\sigma}\sum_{n=1}^{\infty}\frac{A_n}{2n(2n+1)-2}P_{2n}(\cos\theta)$$

$$+\sum_{n=1}^{\infty}C_nP_{2n}(\cos\theta). \quad (26)$$

Now, $\cos\theta$ is expanded into a series of Legendre polynomial $P_{2n}(\cos\theta)$ as [40]

$$\cos\theta=\sum_{n=1}^{\infty}\alpha_nP_{2n}(\cos\theta), \quad (27)$$

$$\alpha_n=\frac{(-1)^{n-1}(2n)!(4n+1)}{2^{2n+1}n!(n+1)!(2n-1)}. \quad (28)$$

Inducing from Eq. (11) yields

$$\bar{\zeta}(\theta,t)=\sum_{n=1}^{\infty}\frac{2nA_n}{i\omega a}P_{2n}(\cos\theta). \quad (29)$$

Substituting Eq. (27) into Eq. (26) and comparing the coefficients with Eq. (29), we have

$$i\omega a\alpha_nA_0+A_n\left\{\frac{\rho a^3\omega^2}{\sigma}\frac{1}{[2n(2n+1)-2]}-2n\right\}=-i\omega aC_n. \quad (30)$$

The anchored condition yields

$$\sum_{n=1}^{\infty}\frac{2nA_n}{i\omega a}P_{2n}(0)=0. \quad (31)$$

Here

$$P_{2n}(0)=\frac{(-1)^n(2n)!}{2^{2n}(n!)^2}. \quad (32)$$

Then,

$$\sum_{n=1}^{\infty}\frac{2nA_n}{i\omega a}\frac{(-1)^n(2n)!}{2^{2n}(n!)^2}=0. \quad (33)$$

All series above are truncated to 20 terms based on test of accuracy and convergence rate. At every time step, an initial meniscus shape is assumed for calculating the electric field distribution. The coefficient B_k is calculated by using Eqs. (10) and (16). The initial meniscus shape is assumed to be a hemisphere. The normal electric field on the meniscus is calculated and substituted into Eq. (25) to get the unknown coefficient C_n. The coefficient A_n is obtained by solving Eqs. (30) and (33). This process is repeated until the convergence criterion is satisfied.

Figure 4 shows the comparison between the theoretical and the experimental meniscus shapes at the beginning and at the end of one oscillation period. Figures 4(a) and 4(b) are the theoretical results of the meniscus shape at the beginning and at the end of the oscillation, showing the contours of the electrical potential. Figures 4(c) and 4(d) are the experimental meniscus shapes at the beginning and at the end of the oscillation. The applied frequency in both the experiment and the simulation was 110 Hz. The liquid used in the experiment was 1 M KCl aqueous solution. It has the surface tension of 73.97 mN/m. However, it should be noted that the surface tension reduces according to electric field [41]. Therefore, in this simulation, the surface tension of 50 mN/m is used according to the applied voltage of 4 kV_{peak}. And a uniform electric field of 6×10^5 V/m is used in the simulation. The simulation result shows a good agreement with the experimental result. Therefore, this approach to simulating the droplet oscillation can be further applied to the parametric study of droplet behavior on a plate and extended to the problem of meniscus behavior on the tip of a nozzle.

2. Meniscus oscillation with jetting

In the balanced state of oscillation without jetting, the Maxwell stress concentrated on the antimodes of the meniscus will be balanced with the surface-tension force. This force can maintain the oscillation shape. When the applied voltage increases over an appropriate range for oscillation, the balanced state is broken and droplet ejection takes place. The oscillation behavior of the meniscus with jetting and without jetting is different. Figure 5 shows the instantaneous shapes of the meniscus during one period of applied ac voltage for applied frequencies of 59 and 800 Hz when jetting does and does not occur. At the resonant frequency for mode 2 without jetting, $f=59$ Hz, the meniscus oscillates up and down axisymmetrically. When the applied voltage is increased to 15.5 kVp-p, the electrical stress exceeds the surface-tension force and the balance of oscillation is broken. The meniscus oscillates to the left and right consecutively while applying the ac voltage. Ejection occurs at the apex of the meniscus corresponding to the moment when the applied ac voltage is at positive or negative peaks. In Fig. 5(b), jet-
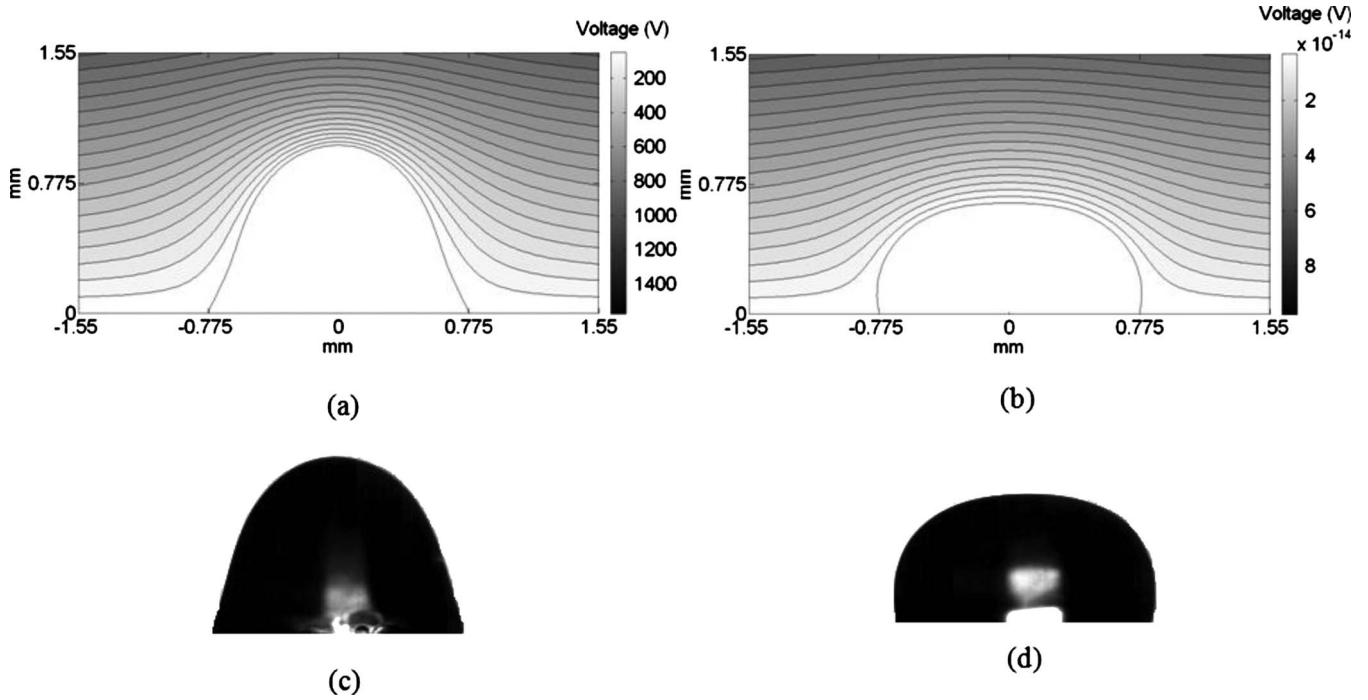
FIG. 4. Comparison of the theoretical and the experimental meniscus shapes at $f=110$ Hz and $E_0=6\times10^5$ V/m.

ting occurs when the meniscus oscillates to the left. The jet is not axisymmetric. Figure 5(c) shows that the meniscus oscillates at a frequency of 800 Hz and at a voltage amplitude of 14.5 kVp-p. Additionally, the shape is asymmetric and the meniscus oscillates to the left and right. However, when the amplitude of the voltage is increased to 15.5 kVp-p, as shown in Fig. 5(d), the phase of the left and the right oscillations is coincident, the oscillation becomes symmetric, and the jetting occurs with the periodic ejection.

Even with dc voltage, oscillation and pulsed jets can also occur [42,43]. Two types of pulsation processes are distinguished: low-frequency fluctuation and high-frequency droplet formation. The low-frequency pulsation is caused by an imbalance between the flow rate supplying liquid to the Taylor cone and the emission rate of the liquid. The high-frequency pulsation mainly results from the initial droplet formation process; it is modulated by the low-frequency pulsation. The oscillation without jetting and the pulsed jet take place in mode 2 when using dc voltage. Their meniscus shapes are similar to those when using ac voltage in mode 2 at low frequency. The oscillation without jetting happens when the applied dc voltage is not strong enough for forming a jet. The effect of ac voltage on the meniscus oscillation and the jetting is more distinguished at high frequency, showing behavior of higher modes such as modes 4, 6, and 8.

Figure 6 shows oscillation and jetting images of the meniscus at 800 Hz with various voltage amplitudes. Each image was produced by superimposing two meniscus shapes at the beginning and at the end of one period. In this case, the distance between the nozzle and the ground electrode is 11 mm. When the applied voltage is larger than a critical value for the jetting, the meniscus oscillates and the jetting occurs periodically as shown in Fig. 6. When the meniscus has an adequate energy accumulated from the applied voltage, the

oscillation mode will change to the jetting mode. After one period of oscillation and jetting, the meniscus oscillates again and starts an oscillation-jetting period. When the applied voltage is increased, the oscillation time during one period becomes shorter and the jetting period becomes
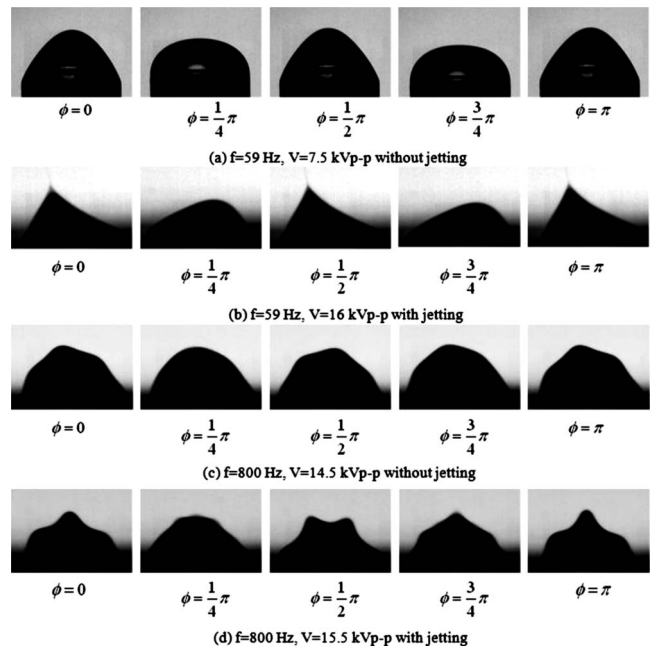

FIG. 5. The meniscus shapes during one period of applied ac voltage: (a) meniscus oscillation without jetting at an applied frequency of 59 Hz, (b) meniscus oscillation with jetting at an applied frequency of 59 Hz, (c) meniscus oscillation without jetting at an applied frequency of 800 Hz, and (d) meniscus oscillation with jetting at an applied frequency of 800 Hz.
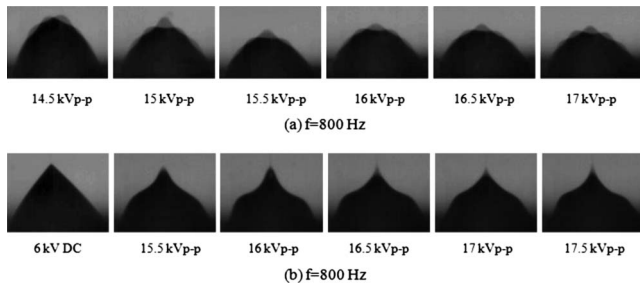
FIG. 6. Jetting and meniscus oscillation: (a) meniscus oscillation according to applied ac voltages at 800 Hz. (b) Jets under 6 kV dc voltage and various amplitude ac voltages from 15.5 to 17.5 kVp-p at 800 Hz.

longer. This indicates that the accumulated energy is sufficient to induce jetting more easily. The applied frequency of 800 Hz is in the range of oscillation mode 6. Figure 7 shows the behavior of the meniscus according to the applied frequency under an amplitude of 16 kVp-p. The ejection of liquid occurs more readily at a lower frequency than at a higher frequency at the same applied voltage for various frequencies. There is no oscillation time prior to jetting for the cases with a frequency of less than 90 Hz. The oscillation is shown at 90 Hz; its time within one period increases when the frequency exceeds 90 Hz. This indicates that the energy supplied to the meniscus in one period of ac voltage is inversely proportional to the applied frequency.

A resonantly axisymmetric jet was observed. For the oscillation without jetting, the resonant frequencies are 59, 399, and 610 Hz corresponding to modes 2, 4, and 6, respectively, while, for jetting, they are shifted to 90, 500, and 800 Hz. The volume of the fluid in the meniscus of oscillation without jetting is unchanged; hence, the oscillation is very stable at each resonant frequency. However, in the jetting case, the liquid is supplied to the meniscus by pumping and is removed by ejection. Therefore, the meniscus behavior is more complex than that the case for the pure oscillation without jetting. At a frequency of 90 Hz, jetting occurs regularly at every ac signal peak. The meniscus moves up and down. At the end of the upward movement, jetting occurs. However, at frequencies of 500 and 800 Hz, the meniscus oscillates in a finite period; subsequently, a finite period of jetting occurs. This process occurs continually. Specifying resonant modes in the jetting case is based on the observation of the resonant mode of oscillation in the oscillating period. Due to the disturbance of the ejection, the meniscus must relax in a finite oscillation period for stabilization before commencing with
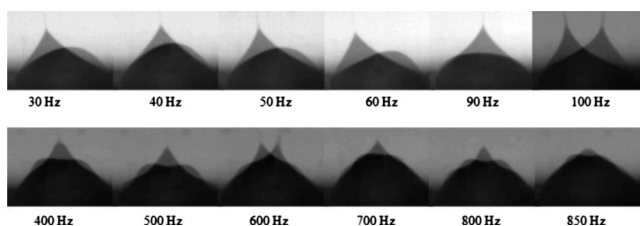

FIG. 7. Jets at 16 kVp-p ac voltage with various frequencies from 30 to 850 Hz.

jetting. As the mode becomes higher, the disturbance increases. Hence, the oscillation period is longer at a higher mode, as in the present observation.

Table I shows that the oscillation frequency of the meniscus is twofold greater than the applied frequency when the latter is less than 100 Hz and is equal to the applied frequency when it is larger than 100 Hz; thus, 100 Hz was deemed to be the critical frequency. This is most likely attributed to a reduction in the electrical energy supplied to the meniscus according to increases in the applied frequency.

B. Effect of ac voltage superimposed on dc voltage

Figure 8(a) shows the meniscus shapes under dc voltage superimposed by ac voltage signals from 1 to 8 kVp-p. Each image is produced by superimposing two meniscus shapes at the beginning and at the end of one period. The distance between the nozzle and the ground electrode is 8 mm. A bias dc voltage of 5 kV is superimposed by ac voltage with a frequency of 800 Hz. The experimental results indicate that the cone jet appears when the ac voltage is low and the dc voltage is dominant, which is very similar to the conditions for a Taylor cone jet under 5 kV of dc voltage, as shown in Fig. 8(b). The meniscus only oscillates up and down. At the end of the upward movement, the meniscus gains sufficient electric stress and jetting occurs. When the applied ac voltage is higher than 5 kVp-p, which is equal to the bias dc voltage, the behavior of the meniscus becomes similar to that associated with the ac voltage. The meniscus oscillates periodically and jetting takes place when the meniscus arrives at the highest point.

Hayati *et al.* [44] suggested that, during spraying, the electric field within the liquid will drive the free charge to the surface of the cone; hence, the surface will become charged and is subjected to the normal electrical field E_n. Due to the finite conducting nature of the liquid, a voltage difference will exist between the base of the cone at the end of the capillary and the tip of the cone. This voltage difference ensures that the interface is subjected to a tangential electric field E_t in the direction of the flow. Therefore, the tangential electrical stress on the cone becomes

$$\tau_t = \varepsilon_0 E_t E_n, \tag{34}$$

where ε_0 is the permittivity of free space and $\varepsilon_0 E_n$ describes the surface charge.

For the dominant dc voltage zone in the present experiment, when the applied voltage is at the upper peak, the meniscus is sharp and elongated. The normal and the tangential electric fields then increase. Accordingly, the tangential electrical stress increases [Eq. (34)]. This stress induces a stronger backflow at the meniscus center, which reserves of the most liquid in the meniscus. As a result, only a thin liquid layer is moved to the tip of the meniscus, where it is ejected as a thin jet. A convex cone then forms. Therefore, the jet occurs at the end of the upward movement of the meniscus. In cone-jet mode electrosprays, charges must also be relaxed at the cone-jet surface because the motion of the charges inside the liquid bulk would result in incompatibility as regard the steadiness of the cone-jet mode. Consequently, the

TABLE I. Meniscus oscillation frequency according to applied ac voltage frequency and amplitude.

Applied ac frequency (Hz)		30	40	60	90	100	300	600	700	800
	14 kVp-p	60	80	120	180	100	300	600	700	800
Oscillation	14.5 kVp-p	60	80	120	180	100	300	600	700	800
frequency	15 kVp-p	60	80	120	180	100	300	600	700	800
	16 kVp-p	60	80	120	180	100	300	600	700	800

electrical relaxation time must be short compared to hydrodynamic time in electrospray atomization [3]. In the present case, at the moment the jet occurs, the jetting is similar to the cone-jet mode because the dc voltage is dominant over the ac voltage. Therefore, the condition of the occurrence of the jet is applicable to this case. The electrical relaxation time $t_e = \beta \varepsilon_0 / K$ for ethanol with a conductivity of $K = 0.0013$ μS/cm and a dielectric constant of $\beta = 24.3$ is $t_e = 1.65 \times 10^{-3}$ s. The hydrodynamic time $t_h = LR^2/Q$ with an axial characteristic jet length of $L = 1$ mm, a radial characteristic jet length of $R = 40$ μm, and a flow rate of $Q = 3$ μl/min is $t_h = 3.2 \times 10^{-2}$ s. The period of the applied frequency of 800 Hz is $T = 1.25 \times 10^{-3}$ s. The electrical relaxation time is shorter than the hydrodynamic time and on the same order as the period of the applied frequency. This relaxation time ensures that the charge in the bulk liquid is relaxed, satisfying the condition of the formation of jetting.

C. Effect of pulsed dc voltage

In previous studies [19,20], a pulsed dc voltage was used for the drop-on-demand operation of jetting droplets. In this study, the meniscus behavior and the jetting characteristics are compared at the aforementioned ac voltage or with the ac voltage superimposed on the dc voltage. The bias voltage was fixed at 5 kV and pulsed voltage was varied from 0.5 to 3 kV. Figure 8(b) shows that the meniscus and the jet are similar to those when the dc voltage is coupled with ac voltage and the ac amplitude is lower than 5 kVp-p. The heights of the cone and the relaxed meniscus in one period were measured as shown in Fig. 9. For the pulsed dc case, the cone and the relaxed meniscus heights are slightly decreased according to an increasing pulse voltage. The difference between the cone and the meniscus heights is mostly unchanged as the dc bias voltage is dominant over the pulsed voltage. However, for jetting under ac voltage superimposed on dc bias voltage, the cone height increases and the relaxed meniscus decreases according to increases in the ac voltage. This trend differs from the case of pulsed dc voltage. As the ac voltage is increased, its effect becomes dominant and the oscillation mode follows the ac mode shown in Figs. 6 and 7. When the ac voltage becomes 5 kVp-p, the height suddenly decreases due to the ac mode of oscillation. The meniscus is not elongated. Therefore, a large decrease in the meniscus height becomes evident when the ac voltage is larger than the bias voltage. The difference between the cone and the meniscus heights increases according to the ac voltage.

D. Discussion

Interestingly, it was found that the droplet ejection and the meniscus oscillation frequencies are twice the applied frequency when the latter is less than 120 Hz. However, the droplet ejection and the meniscus oscillation frequencies are equal to the applied frequency when the applied frequency is higher than 120 Hz as presented in Table I. Table II shows the jetting frequencies under 5 kV of dc voltage (positive) superimposed by ac voltages. The ejection could happen only at the positive peak of the ac signal because the superimposed voltage should be higher than the typical value to cause the ejection. Therefore, the jetting frequencies should be the same as the applied frequency. However, a trend similar to that of the meniscus oscillation frequency was observed according to the applied frequency of ac voltages. As shown in Table II, the jetting frequencies are equal to the applied frequency when the latter is less than 100 Hz, while the jetting frequencies are half of the applied frequency when the applied frequency is higher than 100 Hz. There is a sudden change in the relationship between the jetting or the meniscus oscillation frequency and applied frequency when the applied frequency is greater or less than a critical value.

The electric field drives the free charge to the surface of the meniscus and, hence, the surface will become charged and is subjected to the electrical force. The resultant force induces the oscillation of the meniscus and the ejection of the droplets. When one considers the energy conservation law, this electrical energy is converted to mechanical energy for the oscillation or the ejection. Therefore, the change in oscillation or jetting frequency is related to the energy conservation and may be explained by the electrical energy level imposed on the liquid meniscus. This phenomenon of reduction in the jetting or the oscillation frequency is most likely due to the insufficient electrical energy supplied to the liquid meniscus when the applied frequency increases. In the present experiment, the applied ac voltage is a harmonic function, i.e., given as

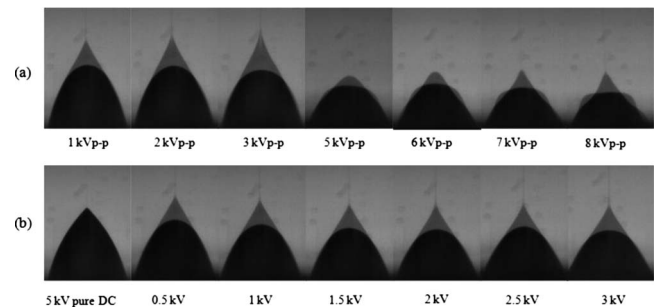$$V(t) = \sqrt{2} V_{rms} \sin(\omega t), \tag{35}$$

FIG. 8. Jetting and meniscus oscillation: (a) meniscus oscillations and jets under 5 kV dc voltage superimposed by various ac voltages from 1 to 8 kVp-p. (b) Jet at 5 kV dc voltage and pulsed dc voltage with a bias voltage of 5 kV and a pulse from 0.5 to 3 kV.
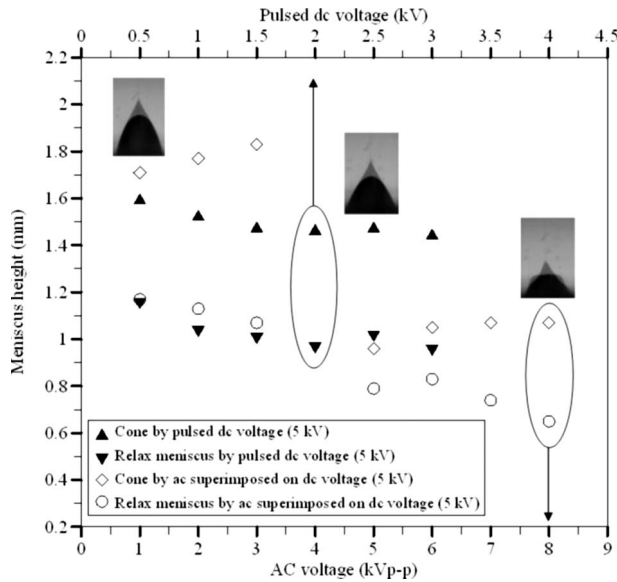
FIG. 9. Meniscus heights under pulsed dc voltage and ac voltage superimposed on dc voltage.

where the subscript *rms* means the root mean square, ω is frequency, and t is time. The current in the circuit is given as

$$I(t) = \sqrt{2} I_{rms} \sin(\omega t - \theta), \tag{36}$$

where θ is the phase angle. The energy of the ac voltage in 1 cycle is then given as

$$E = T V_{rms} I_{rms} \cos \theta, \tag{37}$$

where T is the period.

Equation (37) notes that the electrical energy supplied to the liquid meniscus is proportional to the period and the average voltage and current. As the applied frequency is increased, the period becomes smaller. Therefore, the electrical energy is inversely proportional to the applied frequency. When the applied frequency is low, the electrical energy is sufficient to eject the droplet or oscillate the meniscus at every peak during 1 cycle. However, when the applied frequency exceeds the critical value, the electrical energy decreases and cannot sufficiently conduct two jets or oscillations per cycle as shown in Fig. 10(b). At the lower (minus) peak of the ac signal, jetting cannot occur. Therefore, the oscillation frequency should be equal to the applied frequency and the jetting frequency should be half of the applied frequency as shown in Tables I and II.

Kweon *et al.* [45] reported a similar phenomenon for the oscillation frequency of a bubble located on a needle under an ac electric field in cyclohexane according to the applied frequency. They noted that there is a critical applied voltage for the transient rising of the bubble oscillation frequency. If

TABLE II. Jetting frequencies under an ac voltage of 5 kVp-p superimposed on dc voltage with various frequencies (5 kV).

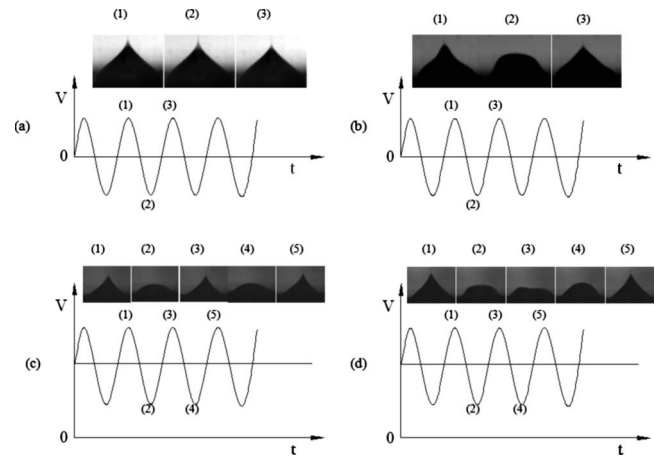| Applied ac frequency (Hz)	60	120	400	800
Jetting frequency (Hz)	60	120	200	400

FIG. 10. Jetting frequency according to applied frequency: (a) sequential images of menisci at an ac voltage of 16 kVp-p with 90 Hz, (b) sequential images of menisci at an ac voltage of 16 kVp-p with 400 Hz, (c) sequential images of menisci at an ac voltage of 8 kVp-p with 120 Hz superimposed on a dc voltage of 5 kV, and (d) sequential images of menisci at an ac voltage of 8 kVp-p with 400 Hz superimposed on a dc voltage of 5 kV.

the applied voltage is less than the critical value, the oscillation is equal to the applied frequency. If the applied voltage is larger than the critical value, the oscillation is two times higher than the applied frequency. This phenomenon may also be explained by Eq. (37). When the voltage is increased, the electrical energy must be increased until it is sufficient to allow two oscillations per cycle. This result also consolidates the present hypothesis to explain the findings of this study. Figure 10 shows sequential images of meniscus shapes according to the applied signal of the ac voltage or ac voltage superimposed on dc voltage. For the ac voltage signal at a low frequency, jetting occurs at every peak of the applied voltage [Fig. 10(a)]. For the dc voltage case, after charge relaxation, diffuse-layer-type polarization is generated due to the liquid electric field, and the charge can be focused by interfacial singularities such as sharp cones. At low ac voltage frequencies, liquid phase charge separation and accumulation behavior, analogous to the dc case, are possible and droplets can be excited according to both positive and negative peaks of the voltage signal. Hence, the jetting frequency is greater by twofold compared to the applied frequency. For ac voltage superimposed on dc voltage, at a low ac voltage frequency, the jet occurs at every upper peak [Fig. 10(c)]. At the lower peak, the electric force is not sufficient to form a jet. Hence, the jetting frequency is equal to the applied frequency. However, at a higher applied frequency than the critical value, the energy of the meniscus in one period decreases. The energy should be accumulated in 2 cycles to reach the critical value for the formation of the jet [Fig. 10(d)]. Consequently, the jetting frequency is half of the applied frequency. In this study, it was found that the critical frequencies for oscillation and jetting by ac voltage and ac voltage superimposed on dc voltage are 100 and 120 Hz, respectively. Based on this investigation of the effects of voltage signals on the oscillation and the jetting of a liquid, a EHD inkjet printing device was designed and proposed.

IV. CONCLUSION

This study experimentally investigated meniscus oscillation and jetting under ac voltage, ac voltage superimposed on dc voltage, and pulsed dc voltage. Conclusions are as follows:

(1) For applied ac voltage, jetting occurs at the end of an oscillation cycle where the meniscus oscillates upward and arrives at the highest position. Furthermore, the oscillation frequency of the meniscus may be double or equal to the applied frequency when the applied frequency is less than or larger than the critical frequency (100 Hz), respectively.

(2) For ac voltage superimposed on dc voltage, when the applied ac signal is less than the dc voltage, the jetting behavior is similar to that of a Taylor cone jet. However, when the applied ac signal is larger than the dc voltage, the meniscus behavior is similar to that under ac voltage. Furthermore, the oscillation frequency of the meniscus is equal to or half

that of the applied frequency when the applied frequency is less than or larger than the critical frequency (120 Hz), respectively. Using ac voltage or ac voltage superimposed on dc voltage, tiny droplets applicable to an EHD inkjet print head can be generated.

(3) For pulsed dc voltage, the meniscus behavior does not change much even when the applied pulse amplitude increases. Using this signal, a conventional EHD inkjet head was developed for drop-on-demand operations.

ACKNOWLEDGMENTS

[1] J. Zeleny, Phys. Rev. **10**, 1 (1917).
[2] G. Taylor, Proc. R. Soc. London, Ser. A **280**, 383 (1964).
[3] A. M. Gañán-Calvo, J. Dávila, and A. Barrero, J. Aerosol Sci. **28**, 249 (1997).
[4] M. Cloupeau and B. Prunet-Foch, J. Electrost. **25**, 165 (1990).
[5] R. P. A. Hartman, J.-P. Borra, D. J. Brunner, J. C. M. Marijnissen, and B. Scarlett, J. Electrost. **47**, 143 (1999).
[6] R. P. A. Hartman, J.-P. Borra, D. J. Brunner, D. M. A. Camelot, J. C. M. Marijnissen, and B. Scarlett, J. Aerosol Sci. **30**, 823 (1999).
[7] R. P. A. Hartman, D. J. Brunner, D. M. A. Camelot, J. C. M. Marijnissen, and B. Scarlett, J. Aerosol Sci. **31**, 65 (2000).
[8] A. Jaworek, W. Machowski, A. Krupa, and W. Baiachandran, Industry Applications Conference **2**, 770 (2000).
[9] B. Quang Tran Si, D. Byun, and S. Lee, J. Aerosol Sci. **38**, 924 (2007).
[10] D. Byun, Y. Lee, S. B. Q. Tran, V. D. Nguyen, S. Kim, B. Park, S. Lee, N. Inamdar, and H. H. Bau, Appl. Phys. Lett. **92**, 093507 (2008).
[11] A. G. Bailey and J. E. Bracher, J. Spacecr. Rockets **9**, 518 (1972).
[12] J. Xiong, Z. Zhou, D. Sun, and X. Ye, Sens. Actuators, A **117**, 168 (2005).
[13] L. F. Velasquez-Garcia, A. I. Akinwande, and M. Martinez-Sanchez, J. Microelectromech. Syst. **15**, 1260 (2006).
[14] J. B. Fenn, M. Mann, C. K. Meng, S. K. Wong, and C. Whitehouse, Science **246**, 64 (1989).
[15] P. Griss, J. Melin, J. Sjõdahl, J. Roeraade, and G. Stemme, J. Micromech. Microeng. **12**, 682 (2002).
[16] G. A. Schultz, T. N. Corso, S. J. Prosser, and S. Zhang, Anal. Chem. **72**, 4058 (2000).
[17] K. Hakiai, Y. Ishida, A. Baba, and T. Asano, Jpn. J. Appl. Phys., Part 1 **44**, 5781 (2005).
[18] J. U. Park, M. Hardy, S. J. Kang, K. Barton, K. Adair, D. K. Mukhopadhyay, C. Y. Lee, M. S. Strano, A. G. Alleyne, J. G. Georgiadis, P. M. Ferreira, and J. A. Rogers, Nature Mater. **6**, 782 (2007).

[19] D. Y. Lee, Y. S. Shin, S. E. Park, T. U. Yu, and J. H. Hwang, Appl. Phys. Lett. **90**, 081905 (2007).
[20] S. Lee, D. Byun, D. Jung, J. Choi, Y. Kim, J. H. Yang, S. U. Son, S. B. Q. Tran, and H. S. Ko, Sens. Actuators, A **141**, 506 (2008).
[21] J. Choi, Y. J. Kim, S. Lee, S. U. Son, H. S. Ko, V. D. Nguyen, and D. Byun, Appl. Phys. Lett. **93**, 193508 (2008).
[22] R. Pareta and M. J. Edirisinghe, J. R. Soc., Interface **3**, 573 (2006).
[23] S. N. Jayasinghe, A. N. Qureshi, and P. A. M. Eagles, Small **2**, 216 (2006).
[24] K. L. Choy and B. Su, Thin Solid Films **388**, 9 (2001).
[25] S. N. Reznik, A. L. Yarin, A. Theron, and E. Zussman, J. Fluid Mech. **516**, 349 (2004).
[26] G. H. Kim and J. H. Park, Appl. Phys. A: Mater. Sci. Process. **86**, 347 (2007).
[27] S. Sarkar, N. Levit, and G. Tepper, Sens. Actuators B **114**, 756 (2006).
[28] S. Sample and R. Bollini, J. Colloid Interface Sci. **41**, 185 (1972).
[29] M. Sato, J. Electrost. **15**, 237 (1984).
[30] Z. Huneiti, W. Balachandran, and W. Machowski, J. Electrost. **40-41**, 97 (1997).
[31] D. Lastochkin and H. C. Chang, J. Appl. Phys. **97**, 123309 (2005).
[32] S. Maheshwari and H. C. Chang, Appl. Phys. Lett. **89**, 234103 (2006).
[33] S. Maheshwari and H. C. Chang, J. Appl. Phys. **102**, 034902 (2007).
[34] Lesliey Yeo, Dimitri Lastochkin, Shau-Chun Wang, and Hsueh-Chia Chang, Phys. Rev. Lett. **92**, 133902 (2004).
[35] J. M. Oh, S. H. Ko, and K. H. Kang, Langmuir **24**, 8379 (2008).
[36] Ping Wang, Siddharth Maheshwari, and Hsueh-Chia Chang, Phys. Rev. Lett. **96**, 254502 (2006).
[37] M. Strani and F. Sabetta, J. Fluid Mech. **141**, 233 (1984).
[38] M. Strani, Meccanica **21**, 15 (1986).

[39] E. De Bernardis and M. Strani, J. Sound Vib. **122**, 523 (1988).

[40] H. F. Bauer Arch. Appl. Mech. **62**, 517 (1992).

[41] M. Sato, N. Kudo, and M. Saito, IEEE Trans. Ind. Appl. **34**, 294 (1998).

[42] R. Juraschek and F. W. Röllgen, Int. J. Mass. Spectrom. **177**, 1 (1998).

[43] J. Wei, W. Shui, F. Zhou, Y. Lu, K. Chen, G. Xu, and P. Yang, Mass Spectrom. Rev. **21**, 148 (2002).

[44] I. Hayati, A. Bailey, and T. F. Tadros, Nature (London) **319**, 41 (1986).

[45] Y. C. Kweon, M. H. Kim, H. J. Cho, and I. S. Kang, Int. J. Multiphase Flow **24**, 145 (1998).